

Creep performance of concrete-filled steel tubular (CFST) columns and applications to a CFST arch bridge

Meng-Gang Yang ^{*1}, C.S. Cai ² and Yong Chen ³

¹ School of Civil Engineering, Central South University, Changsha 410075, P.R. China

² Department of Civil and Environmental Engineering,
Louisiana State University, Baton Rouge, Louisiana 70803, USA

³ Shanghai Municipal Engineering Design Institute (Group) Co. Ltd., Shanghai 200092, P.R. China

(Received February 28, 2014, Revised December 01, 2014, Accepted December 26, 2014)

Abstract. This paper first presents an experimental study of twelve specimens for their creep performance, including nine concrete-filled steel tubular (CFST) columns and three plain concrete columns, subjected to three levels of sustained axial loads for 1710 days. Then, the creep strain curves are predicted from the existing creep models including the ACI 209 model, the MC 78 model, and the MC 90 model, and further a fitted creep model is obtained by experimental data. Finally, the creep effects of a CFST arch bridge are analyzed to compare the accuracy of the existing creep models. The experimental results show that the creep strains in CFST specimens are far less than in the plain concrete specimens and still increase after two years. The ACI 209 model outperforms the MC 78 model and the MC 90 model when predicting the creep behavior of the CFST specimens. Analysis results indicate that the creep effects in the CFST arch bridge are significant. The deflections and stresses calculated by the ACI 209 model are the closest to the fitted model in the three existing models, demonstrating that the ACI 209 model can be used for creep analysis of CFST arch bridges and can meet the engineering accuracy requirement when lack of experimental data.

Keywords: Concrete-filled steel tubular (CFST); creep experiment; creep performance; creep effect; CFST arch bridge

1. Introduction

Concrete creep is one of the important factors influencing the mechanical performance of concrete-filled steel tubular (CFST) arch bridges. Previous studies (Shrestha *et al.* 2011, Shao *et al.* 2010, Bradford *et al.* 2011) have shown that the creep of core concrete leads to significant stress redistribution in CFST sections, namely, an increase of stresses of steel tubes and a reduction of compressive stresses of core concrete. Since the core concrete is sealed in steel tubes without humidity exchanging and is also in the three-dimensional state of stress due to the constraint from the steel tubes, the concrete creep in CFST arch bridges is complicated and different from the ordinary reinforced or plain concrete structures. Therefore, it is very necessary to investigate creep performance of CFST columns by creep experiments and recommend a well-predicted existing

*Corresponding author, Professor, E-mail: mgyang@csu.edu.cn

model for creep analysis of CFST arch bridges.

At present, the creep models which are commonly used in creep analysis of CFST structures include the MC 78 model (CEB-FIP 1978), the MC 90 model (CEB-FIP 1990), the ACI 209 model (ACI Committee 209 1992), the GL 2000 model (Gardner and Lockman 2001), and the B3 model (Bazant and Baweja 1995). More experimental tests were carried out to investigate the creep behavior of other different types of concrete, including high-strength concrete (Mazloom 2008, Pan *et al.* 2011), high-performance concrete (Chen and Yuan 2008, Persson 2001), FRP reinforced concrete (Torres *et al.* 2012), and high-early-strength self-consolidating concrete (Kim *et al.* 2011).

There were some experimental studies on creep models for CFST specimens. Ma and Wang (2012) investigated the creep of axially loaded high-strength CFST columns by testing eight specimens for 380 days and developed the creep model of high-strength CFST columns based on the B3 Model. Yang *et al.* (2008) presented the creep experimental patterns on recycled aggregate CFST specimens for about eighteen months. Acar (2007) carried out a test of long-term behavior of CFST columns for 200 days and evaluated the creep coefficient. Wang *et al.* (2011) investigated the accuracy of predicting the long-term response for the four concrete models EC2, MC90, AFREM and B3, based on the experimental studies of eleven CFST column specimens over a period of 5 months. Since all the testing durations in these studies are less than two years, the experimental results need further verification through longer-time tests. In fact, the concrete creep in CFST specimens still continues to develop after two years, which has been verified by the creep experiments in the present study.

Furthermore, the influence of concrete creep on the mechanical behavior of CFST arch bridges had been performed. Shao *et al.* (2010) investigated the time-dependent behavior of a CFST arch bridge with a simplified method that is verified by a scaled (1:5) segmental model experiment. Bradford *et al.* (2011) calculated the time-dependent behavior of CFST circular arches under a sustained uniform radial load by using an algebraically tractable age-adjusted effective modulus method. Ma *et al.* (2011) investigated the influence of concrete creep on the seismic response of CFST arch bridges, based on the B3 creep model. All these previous results indicate that the concrete creep has a considerable influence on the mechanical behavior of CFST arch bridges, and the influence is related to both the structural parameters of CFST arch bridges and the adopted creep model for analysis.

In this paper, firstly the creep experiments of twelve specimens, including nine CFST columns and three plain concrete columns, is investigated for 1710 days and the creep behaviors are observed. Then, three existing creep models including the ACI 209 model, the MC 78 model, and the MC 90 model, are used to predict the creep strain curves of the CFST specimens and compared with experimental curves. Finally, the creep effect of a CFST arch bridge is analyzed to compare the accuracy of the existing models so that the well-predicted model can be recommended for creep analysis of CFST arch bridges.

2. Experimental study

2.1 Description of bridge

The Maocaojie Bridge is a half-through CFST tied arch bridge located in the Yiyang city of Hunan province, China. The layout of the bridge is given in Fig. 1. The bridge has a main span of 368 m and two side spans of 80 m. The arch rise is 71.2 m, and the rise-to-span ratio is 1/5 in the

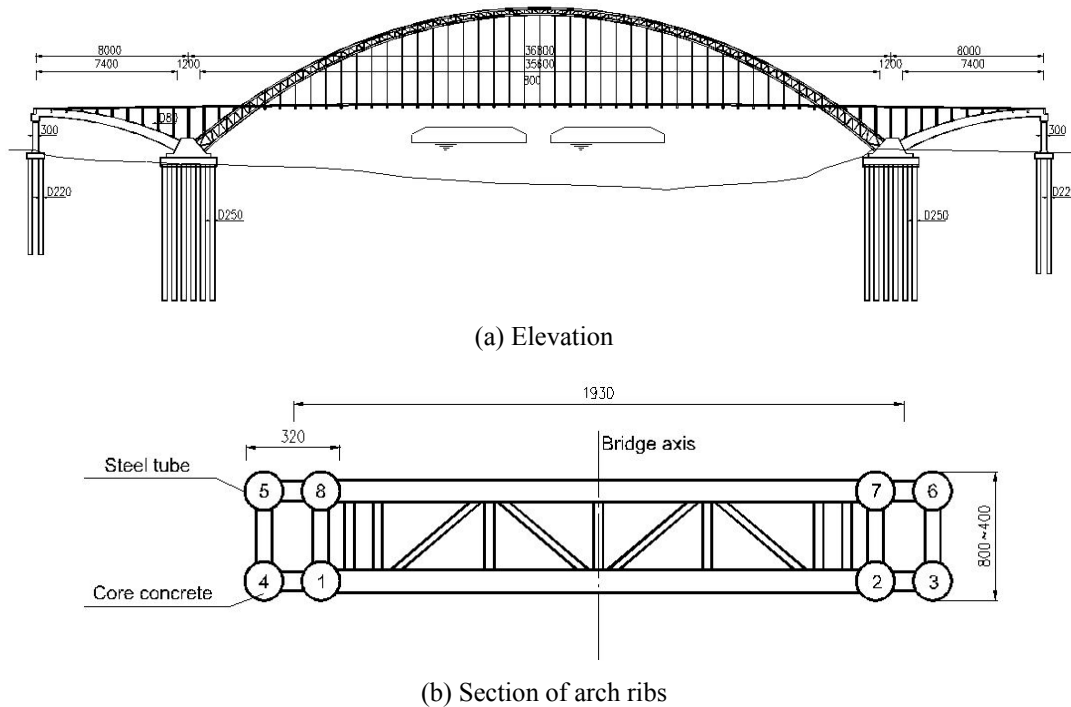


Fig. 1 Layout of Maocaojie Bridge (Unit: cm)

main span. The arch rib line is in a catenary shape, and the coefficient of arch axis is 1.543. The space between the suspenders or the upright columns is 8 m. The bridge has one deck to carry a four-lane highway road. The height of the arch rib varies from 8 m at the arch springing to 4 m at the arch crown, and the center-to-center distance between the two arch ribs is 19.3 m. Each arch rib is composed of four steel tubes, with an outside diameter of 1000 mm and a thickness of 18 mm (increases to 28 mm at the arch springing). The concrete with a designed cube compressive strength of 50 MPa is casted in the steel tubes. Table 1 lists the structural main design parameters of the Maocaojie Bridge.

2.2 Specimen design

A total of sixteen specimens were tested. In these specimens, nine CFST columns and three plain concrete columns were divided into three groups for long-term creep tests subjected to three corresponding levels of sustained axial loads, and the remaining two CFST columns and two plain concrete columns were used for the shrinkage tests which were kept unloaded for the whole duration of the long-term tests. These unloaded specimens have the same materials, age, dimensions and environmental conditions as the loaded ones. The actual creep strains were calculated by subtracting the shrinkage values from the total time-dependent strains of the corresponding specimens under loading. The three levels of sustained loads are 161.6 kN, 202.0 kN and 242.4 kN, corresponding to stress-strength ratios of 0.16, 0.20 and 0.24, respectively. The three ratios can represent three different real states of stress in the arch sections during the Maocaojie Bridge's service and the concrete stress-strength ratios are almost in the range from

Table 1 Structural main design parameters of Maocaojie Bridge

Member		E (kN/m ²)	ρ (kg/m ³)	A (m ²)	I (m ⁴)
Steel tube of arch rib	$\Phi 1000 \times 28$	2.06×10^8	7850	8.55×10^{-2}	101.06×10^{-4}
	$\Phi 1000 \times 22$	2.06×10^8	7850	6.76×10^{-2}	80.36×10^{-4}
	$\Phi 1000 \times 18$	2.06×10^8	7850	5.55×10^{-2}	66.96×10^{-4}
Core concrete of arch rib	$\Phi 1000 \times 28$	3.45×10^7	2550	69.99×10^{-2}	389.31×10^{-4}
	$\Phi 1000 \times 22$	3.45×10^7	2550	71.78×10^{-2}	410.01×10^{-4}
	$\Phi 1000 \times 18$	3.45×10^7	2550	72.98×10^{-2}	423.91×10^{-4}
Upright column	$\Phi 800 \times 12$	2.06×10^8	7850	2.97×10^{-2}	23.06×10^{-4}
Suspender	61 $\Phi^s 7$	2.0×10^8	8392	0.235×10^{-2}	0
Tie	31 $\Phi^l 15.24$	1.9×10^8	8571	0.434×10^{-2}	0
Longitudinal girder		2.06×10^8	7850	7.68×10^{-2}	34.34×10^{-4}

Table 2 Specimens for creep and shrinkage experiments

Test item	Sustained load(kN)	Stress-strength ratio	Type of specimen	Specimen number
Creep	161.6	0.16	CFST	1#, 2#, 3#
			Plain concrete	10#
	202.0	0.20	CFST	4#, 5#, 6#
			Plain concrete	11#
	242.4	0.24	CFST	7#, 8#, 9#
			Plain concrete	12#
Shrinkage	-	-	CFST	13#, 14#
			Plain concrete	15#, 16#

Table 3 Concrete mixing proportion for testing (unit: kg/m³)

Cement	UEA expansion agent	Silica fume	Fine aggregate	Coarse aggregate	Water	FDN water reducing agent
390	48.7	63.3	780	954	185	5.01

0.16 to 0.24. The information of specimens is seen in Table 2. Two types of columns were designed in proportion to the arch rib cross section of the Maocaojie Bridge, and the CFST columns have the same equivalent section area as plain concrete columns to assure the same stress-strength ratio, as illustrated in Fig. 2. The diameter of the plain concrete column specimen is 160 mm, while the outside diameter of the CFST column specimen is 140 mm including the steel tube thickness of 2.5 mm. The height of each specimen is 600 mm. The core concrete with a designed cube compressive strength of 50 MPa is specially designed and made for the Maocaojie Bridge, and the mixing proportion is listed in Table 3.

2.3 Instrumentation and creep test

The dial indicators and the embedded vibrating string extensometers were used to check each other for compressive strain measurements. As for each plain concrete specimen, one vibrating string extensometer was embedded in the center, and two dial indicators were symmetrically installed on the surface of the mid-height section. The measuring-points layout of the CFST specimens was generally similar to that of the plain concrete specimens. The only difference is that there were four dial indicators symmetrically distributed on the outside of the steel tube, and two were for the measurement of the steel tube strain and the other two were for the measurement of the concrete compressive strain. The measuring-points layout is drawn in Fig. 2.

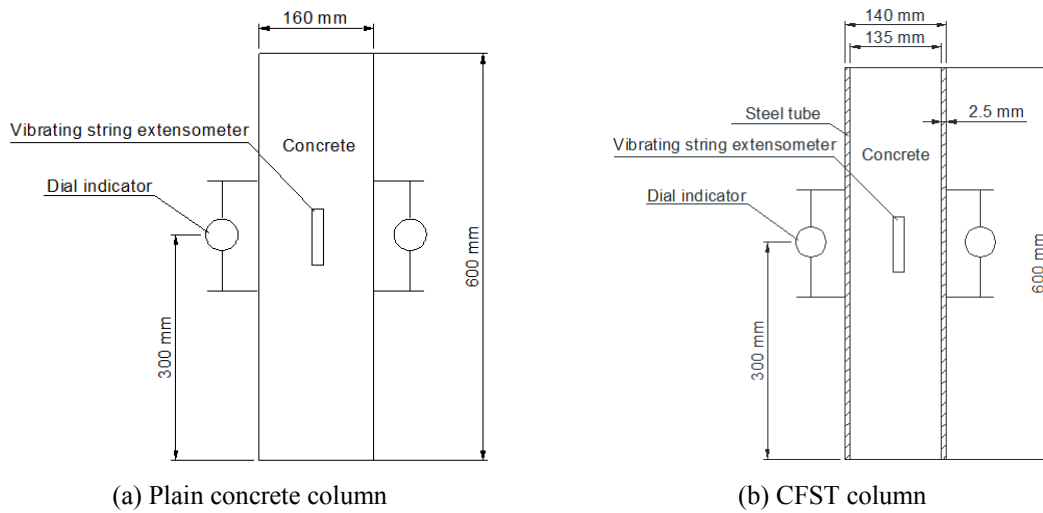


Fig. 2 Design drawing and instrumentation layout



(a) Shrinkage test



(b) Creep test

Fig. 3 Testing equipments and instrumentations for creep experiments

A dedicated creep testing room was established in Central South University, in which an automatic temperature and humidity control system can ensure the specimens under the controlled temperature of $20 \pm 2^\circ\text{C}$ and the relative humidity of 50%~60%. Six creep instruments with the maximum loading of 32 ton were employed for creep test. During the testing process, the creep instruments needed regular adjustments to maintain the sustained load. The testing instrumentations are shown in Fig. 3.

3. Experimental results

3.1 Shrinkage strain

The concrete shrinkage strain curves of two CFST specimens and two plain concrete specimens are depicted in Fig. 4. It can be seen that the shrinkage strains of the plain concrete specimens are far more than those of the CFST specimens, and the ratios of the former to the latter are about 4 by the end of 1710 days. The shrinkage strain of the plain concrete increases rapidly during the first two years, and then becomes stable. For the CFST specimens, the core concrete is in a state of expansion and its shrinkage strain is reverse at the beginning of testing due to the function of UEA expansion agent and the slow water loss inside the steel tube. However, by the time of 200 days the core concrete begins to shrink and its shrinkage strain increases slowly. The lag-and-slow shrinkage can reduce the probability of the core concrete separating from the steel tube and make them work together in CFST arch bridges.

3.2 Creep strain

The concrete creep strain curves of the nine CFST specimens and the three plain concrete specimens subjected to three levels of sustained loads for 1710 days are plotted in Fig. 5. In these curves, the concrete shrinkage strains have been excluded according to Fig. 4. It can be observed that: (i) on one hand, the concrete creep in the CFST specimens and the plain concrete creep have the same trend, including that the creep increases with the increase of the sustained load, the creep

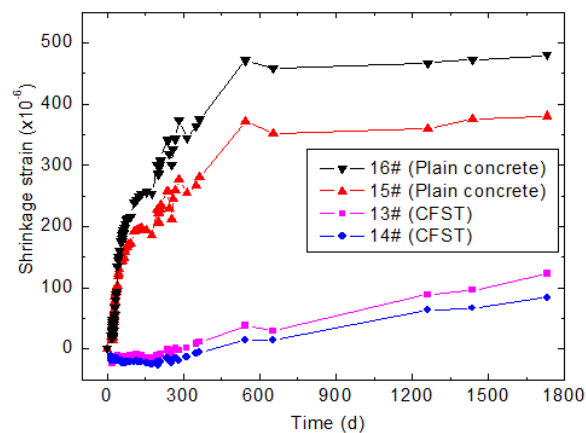
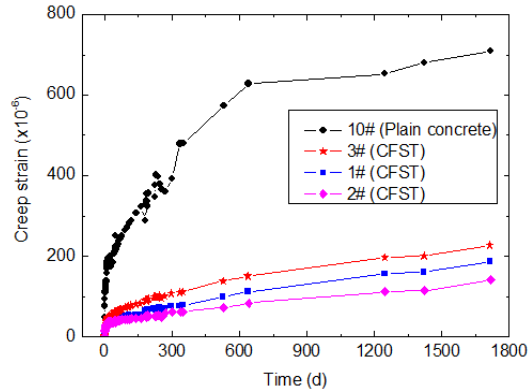
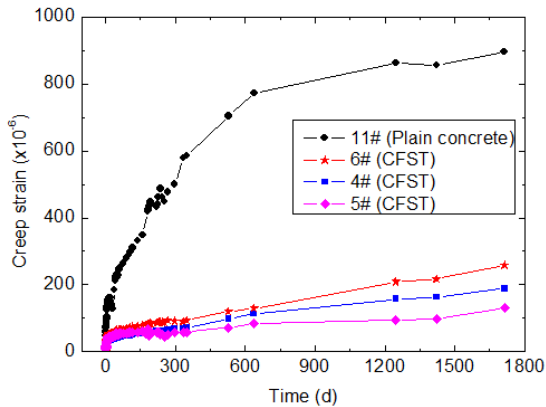


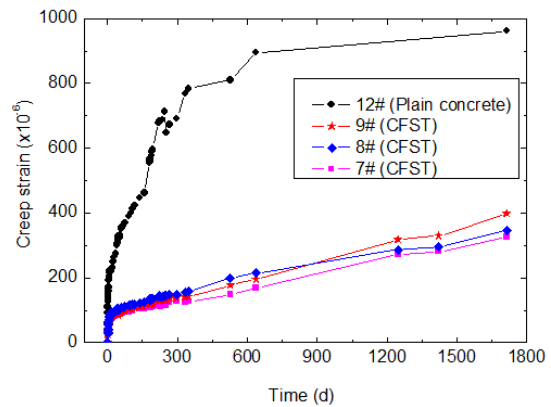
Fig. 4 Experimental shrinkage strain vs. time



(a) Stress-strength ratio 0.16



(b) Stress-strength ratio 0.20



(c) Stress-strength ratio 0.24

Fig. 5 Experimental creep strain vs. time

increases with the increase of loading time, and the creep increases faster at the early stage than at the later stage; (ii) on the other hand, there are some distinctly different creep characteristics between the CFST specimens and the plain concrete specimens. The creep strains of the CFST specimens are far less than those of the plain concrete specimens, and by the end of 1710 days the ratios of the former to the latter are 26.1%, 21.5% and 37.1%, for the three stress-strength ratios 0.16, 0.20 and 0.24, respectively. The plain concrete creep increases rapidly during the first two years, then becomes stable, but the concrete creep in CFST specimens still increases after two years. The plain concrete creep strains by the end of the first two years account for more than 90% of the creep strains measured by the end of the test.

4. Creep prediction of existing models for CFST columns

4.1 Existing creep models

The commonly-used prediction models for concrete creep include the CEB-FIP MC 78 model,

the CEB-FIP MC 90 model, and the ACI 209 model. These models have been adopted in the codes by many countries.

4.1.1 MC 78 model

In the CEB-FIP Model Code 1978 (MC 78 model), the creep strain is composed of the unrecoverable initial plastic strain at loading, the recoverable delayed elastic strain, and the unrecoverable delayed plastic strain after loading. The creep strain is obtained by the linear superposition of them. Therefore, the creep model can be expressed as

$$\phi(t, t_0) = \beta_\alpha(t_0) + \phi_d \beta_d(t - t_0) + \phi_f [\beta_f(t) - \beta_f(t_0)] \quad (1)$$

where $\beta_\alpha(t_0)$ is the unrecoverable initial creep coefficient, $\beta_d(t - t_0)$ is the recoverable delayed elastic coefficient, ϕ_d is the ratio of the delayed elastic strain to initial elastic strain, $\beta_f(t) - \beta_f(t_0)$ denotes the recoverable delayed plastic strain, and ϕ_f is the coefficient with respect to relative humidity and dimensions of the member. Their expressions are

$$\begin{cases} \beta_\alpha(t_0) = 0.8[1 - f_c(t_0)/f_c(\infty)] \\ \beta_d(t - t_0) = 0.73[1 - e^{-0.01(t-t_0)}] + 0.27 \\ \phi_d = 0.4 \\ \beta_f(t) = [t^\alpha / (t^\alpha + \beta)]^{1/3} \\ \phi_f = \phi_{f1} \phi_{f2} \end{cases} \quad (2)$$

where

$$\begin{cases} f_c(t_0)/f_c(\infty) = t_0^{0.73} / (5.27 + t_0^{0.73}) \\ \phi_{f1} = 0.111(0.0002\lambda^3 - 0.043\lambda^2 + 2.57\lambda) - 2.2 \\ \phi_{f2} = 1.12(1 + e^{-0.044h_0^{0.58}}) \\ \alpha = 0.8 + 0.55e^{-0.003h_0} \\ \beta = 770 + 210e^{0.0043h_0} \end{cases} \quad (3)$$

with

$$\begin{cases} h_0 = \gamma(2A_c / u) \\ \gamma = 1.0 + 0.00049e^{0.1\lambda} \end{cases} \quad (4)$$

where A_c is the cross-section (mm^2), u is the perimeter of the member in contact with the atmosphere (mm), and λ is the relative humidity (%).

4.1.2 MC 90 model

In the CEB-FIP Model Code 1990 (MC 90 model), the superposition prediction model of the creep strain was not adopted. Instead, the creep strain was predicted from the product of the notional creep coefficient and a function describing the development of creep with time after

loading. In the notional creep coefficient, the influence patterns of some parameters are taken into account, i.e. compressive strength, age at loading, dimensions of the member, and relative humidity. The creep coefficient of the model can be expressed as

$$\phi(t, t_0) = \phi_0 \beta_c(t - t_0) \quad (5)$$

where ϕ_0 is the notional creep coefficient, β_c is the coefficient to describe the development of creep with time after loading, t and t_0 are the ages of concrete (days) at the moment considered and at loading, respectively. ϕ_0 and β_c can be expressed as

$$\phi_0 = \phi_\lambda \beta(f_{cm}) \beta(t_0) \quad (6)$$

$$\beta_c(t - t_0) = \left[\frac{(t - t_0)}{\beta_H + (t - t_0)} \right]^{0.3} \quad (7)$$

with

$$\begin{cases} \phi_\lambda = 1 + (1 - \lambda) / (0.1h^{1/3}) \\ \beta(f_{cm}) = 16.76 / \sqrt{f_{cm}} \\ \beta(t_0) = 1 / (0.1 + t_0^{0.2}) \\ \beta_H = 1.5 [1 + (1.2\lambda)^{18}] h + 250 \leq 1500 \end{cases} \quad (8)$$

where λ is the relative humidity of the ambient environment (%), h ($= 2A_c / u$) is the average thickness (mm), where A_c is the cross-section and u is the perimeter of the member in contact with the atmosphere, and f_{cm} is the mean compressive strength of concrete at the age of 28 days (MPa).

4.1.3 ACI 209 model

In the ACI 209 model, the creep coefficient was described into the product of a hyperbolic function in term of time and the correction factors of loading age, relative humidity, dimension of the member, slump, fine aggregate percentage and air content, and so on. In this model, the concrete composition is considered, and the creep strain is not divided into delayed elastic strain and plastic strain like the MC 78 model. The creep coefficient of this model can be expressed as

$$\phi(t, t_0) = \frac{(t - t_0)^{0.6}}{10 + (t - t_0)^{0.6}} \phi_u \quad (9)$$

where t_0 is the age of concrete (days) at loading, t is the age of concrete (days) at the moment considered. ϕ_u is the ultimate creep coefficient defined as ratio of creep strain to initial strain and is given by

$$\phi_u = 2.35 \gamma_{la} \gamma_\lambda \gamma_h \gamma_s \gamma_\psi \gamma_\alpha \quad (10)$$

where γ_{la} , γ_λ , γ_h , γ_s , γ_ψ and γ_α are the correction factors of loading age, relative humidity, average thickness, slump, fine aggregate percentage and air content, respectively. These correction factors

can be calculated by the following expressions

$$\begin{cases} \gamma_{la} = 1.25t_0^{-0.118} \\ \gamma_{\lambda} = 1.27 - 0.0067\lambda \\ \gamma_h = 1.10 - 0.00067h \\ \gamma_s = 0.82 + 0.00264s \\ \gamma_{\psi} = 0.88 + 0.0024\psi \\ \gamma_{\alpha} = 0.46 + 0.09\alpha \end{cases} \quad (11)$$

where λ is the relative humidity (%) which should be more than 40, h is the average thickness (mm), s is the observed slump (mm), ψ is the ratio of the fine aggregate to total aggregate by weight (%), and α is the air content (%).

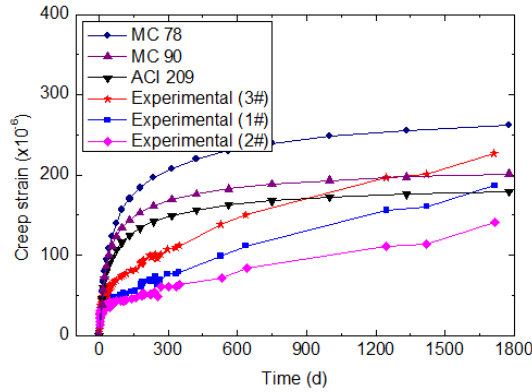
4.2 Comparison between experimental results and predicted ones by existing models for CFST specimens

In the three existing creep models discussed above, there are three very important common parameters that are the age at loading t_0 , the relative humidity λ and the average thickness h . In addition, the mean compressive strength f_{cm} is used for the MC 90 model, and the slump s , the fine aggregate ψ , and the air content α are adopted in the ACI 209 model. In the creep experiment, the values of these parameters are listed in Table 4.

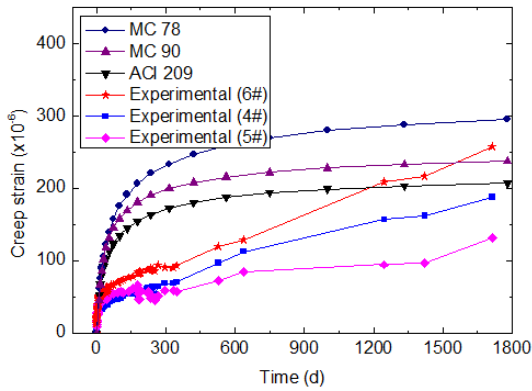
Fig. 6 gives the comparison between the experimental results and the calculated ones by the three models for the CFST specimens subjected to three levels of sustained axial loads. It can be seen that: (i) the creep strain curves predicted from the three models overestimate the creep of the CFST specimens at the early stage although the creep strains at the later stage are close to each other; (ii) the creep strains of the models increase rapidly at the beginning, and then become stable, however the experimental creep strains of the CFST specimens still increase during the testing; (iii) on the whole, there are some discrepancies between the CFST creep strains of the models and the experiment. Since the existing models are obtained by the plain concrete, they cannot fully represent the CFST creep pattern; (iv) in these three models, the creep curve obtained by the ACI 209 model is the closest to the experimental curves of the CFST specimens, indicating that the ACI 209 model outperforms the MC 78 model and the MC 90 model when predicting the creep behavior of the CFST columns.

Table 4 The parameters for the existing creep models

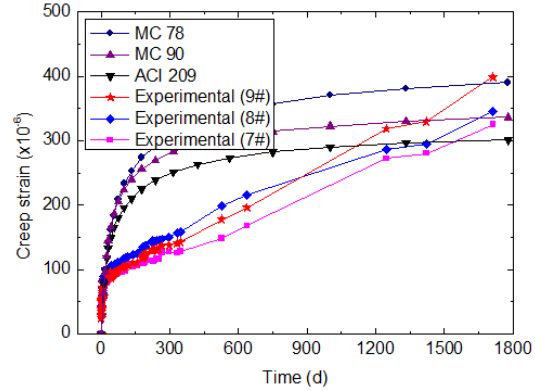
Parameter	Value	Parameter	Value
Age at loading t_0	14 d	Mean compressive strength f_{cm}	53.8 MPa
Relative humidity λ	90%	Slump s	65 mm
Cross-section A_c	14313.9 mm ²	Proportion of fine aggregate Ψ	49.7%
Perimeter u	424.12 mm	Air content α	7.2%
Average thickness $h(=2A_c/u)$	67.5 mm		



(a) Stress-strength ratio 0.16



(b) Stress-strength ratio 0.20



(c) Stress-strength ratio 0.24

Fig. 6 Comparison between experimental results and predicted ones by existing models for CFST specimens

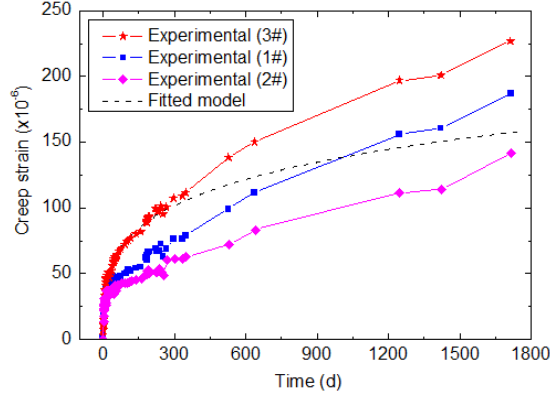
4.3 Fitted model based on ACI 209 model

It can be observed from Fig. 6 that although the creep curve obtained by the ACI 209 model is closer to the experimental curves than the MC 78 and MC 90 models, it does not predict the experimental curves well enough. Therefore, it is necessary to fit the creep model according the experimental results. To make the creep curves calculated by the fitted model not only keep the creep pattern but also agree well with the experimental curves, it is the feasible and efficient way to obtain the fitted model based on the ACI 209 model.

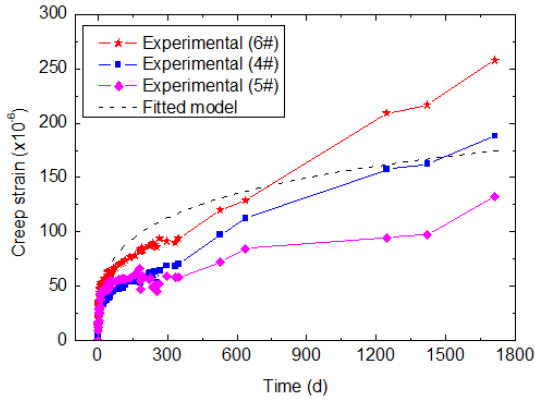
According to Eq. (9), the ACI 209 model can be rewritten as the following expression

$$\phi(t, t_0) = C1 \times \left[\frac{(t - t_0)^{0.6}}{C2 + (t - t_0)^{0.6}} \right] \quad (12)$$

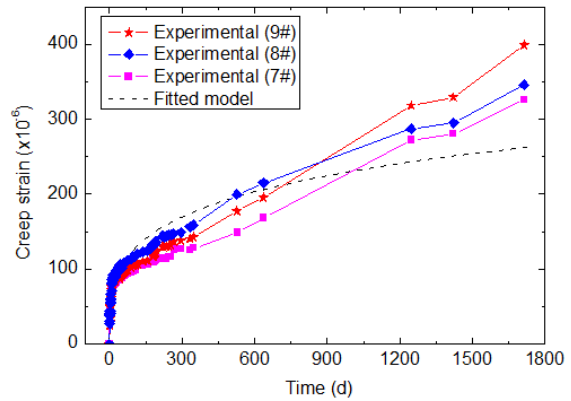
where t_0 is the age of concrete (days) at loading, t is the age of concrete (days) at the moment considered; $C1$ and $C2$ are two undetermined coefficients.



(a) Stress-strength ratio 0.16



(b) Stress-strength ratio 0.20



(c) Stress-strength ratio 0.24

Fig. 7 Predicted creep curves from fitted model for CFST specimens

The least square method is used to fit the coefficients $C1$ and $C2$ based on the experimental data of nine CFST specimens. The fitted model is obtained as

$$\phi(t, t_0) = 1.89432 \times \left[\frac{(t - t_0)^{0.6}}{32.5816 + (t - t_0)^{0.6}} \right] \quad (13)$$

Further, the creep strain curves predicted from the fitted model subjected to the three stress-strength levels are compared with the experimental curves, as shown in Fig. 7. On the whole, the fitted model can represent the creep behavior of the CFST specimens. However, the accuracy of the fitted model decreases with the increase of the sustained load level.

5. Creep effect analysis for a CFST arch bridge

Taking the Maocaojie Bridge as an engineering example, the creep effects of CFST arch bridge

are analyzed with the fitted model, the ACI 209 model, the MC 78 model, and the MC 90 model. In this paper, only the analysis results of steel tube no. 1 (see Fig. 1) are discussed.

5.1 Finite element model

A 3-D finite element model of the Maocaojie Bridge is constructed with the MIDAS software and shown in Fig. 8. In this model, the arch ribs, web members, upright columns, longitudinal girders and cross beams are modeled with spatial beam elements; the suspenders and the ties are modeled with spatial truss elements; the bridge deck is modeled with plate elements; the deck pavement is considered into uniform load. It has been known via static analysis that the skewbacks including the foundations are quite stiff. Thus, the skewbacks are not included in this model and the degrees of freedom associated with these nodes of the skewbacks are restrained.

The whole construction process of the Maocaojie Bridge is simplified into fourteen stages for the creep effect analysis, as listed in Table 5. The number of the eight steel tubes is shown in Fig. 1(b). At the beginning of casting the core concrete of each steel tube, the concrete is regarded as uniform loads acting on the elements of the steel tube. When the compressive strength of the core concrete reaches the design strength, the elements of the core concrete are automatically activated and combined together to work with the steel tube elements. In the MIDAS finite element model, a united material model is used for CFST members, in which two different materials: steel tube and core concrete, are defined to get the respective stress of steel tube and core concrete. Steel tube is treated as elastic material, and the creep model for core concrete is used for the consideration of co-working mechanism of CFST members. The creep effect analysis can be carried out by defining the creep coefficient and the concrete strength curve in MIDAS software.

5.2 Deflection effect

In the creep effect analysis for the Maocaojie Bridge, four different creep models including the fitted model, the ACI 209 model, the MC 78 model, and the MC 90 model, are adopted, and then the results are compared. The step-by-step method is used for creep analysis. The initial time is defined as the time when casting the core concrete of the first steel tube. Thus, the final cumulative time for the creep analysis is 3778 days.

The deflection versus time curves of key sections of the steel tube no. 1 are plotted in Fig. 9. The deflection values at the finished state and at 3650 days after the bridge is finished are listed in

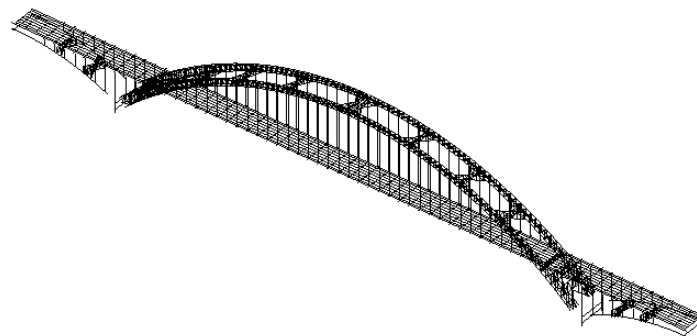


Fig. 8 3-D MIDAS finite element model of the Maocaojie Bridge

Table 5 Construction stages of the Maocaojie Bridge

Stage no.	Content	Stage time (days)	Cumulative time (days)
1	Install the skewbacks, arch ribs, web members, suspenders, longitudinal girders and cross beams	200	200
2	Install the ties and execute their first tension to 26400 kN	6	206
3	Cast the core concrete of steel tube no. 1	6	212
4	Cast the core concrete of steel tube no. 2, then execute the ties' second tension to 34800 kN	6	218
5	Cast the core concrete of steel tube no. 3	6	224
6	Cast the core concrete of steel tube no. 4, then execute the ties' third tension to 43200 kN	6	230
7	Cast the core concrete of steel tube no. 5	6	236
8	Cast the core concrete of steel tube no. 6, then execute the ties' fourth tension to 51600 kN	6	242
9	Cast the core concrete of steel tube no. 7	6	248
10	Cast the core concrete of steel tube no. 8, then execute the ties' fifth tension to 58800 kN	6	254
11	Install half of the deck, then execute the ties' sixth tension to 64800 kN	20	274
12	Install the remaining half of the deck, then execute the ties' seventh tension to 74400 kN	20	294
13	Accomplish the deck paving, then execute the ties' eighth tension to 83600 kN	40	334
14	Service stage	3650	3984

Table 6. In which, “-” denotes the downward deflection. It can be seen that: (i) the deflection of the arch rib increases with the increase of time due to the creep effect of the core concrete; (ii) the creep deflections calculated by the fitted model are less than by the other three creep models, and the results of the ACI 209 model are the closest to the fitted model; (iii) by the end of 3650 days after the bridge is finished, the increase ratio of deflections (i.e., the ratio of the cumulative creep deflection to the deflection without creep) obtained by the fitted model at the arch crown (mid-span) and 1/4-span cross section are 27.1% and 20.8% respectively, which demonstrates that the creep effect of the CFST arch bridge is significant; (iv) the ratios of the creep deflections after the bridge is finished to the cumulative creep deflections are about 40%, thus the deflection induced by the creep after the bridge is finished cannot be neglected; (v) the differences of the increase ratio by creep between the fitted model and the ACI 209 model are 3.5% and 3.7% at the arch crown and 1/4-span cross section respectively, which are less than 5%, demonstrating that the ACI 209 model can be used for creep deflection analysis of CFST structures and can meet the engineering accuracy requirement when lack of experimental data.

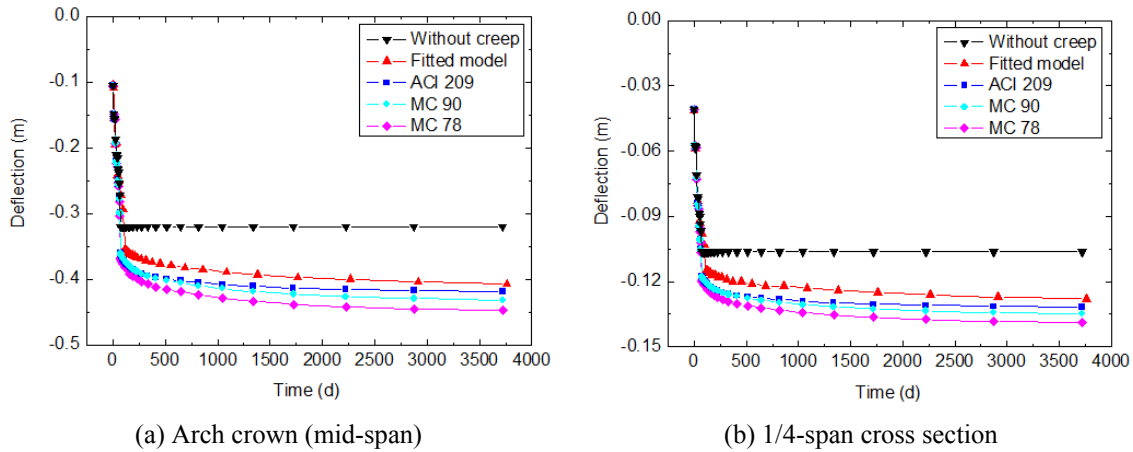


Fig. 9 Deflection curves of key sections of steel tube no. 1

Table 6 Deflections of steel tube no. 1 for different creep models (unit: m)

Section	Creep model	Finished state	Creep deflection after finished	3650 days after finished	Cumulative creep deflection	Increase ratio by creep
Arch crown (mid-span)	Without creep	-0.320	-	-0.320	-	-
	Fitted model	-0.354	-0.034	-0.407	-0.087	27.1%
	ACI 209 model	-0.361	-0.041	-0.418	-0.098	30.6%
	MC 90 model	-0.360	-0.040	-0.432	-0.112	35.0%
	MC 78 model	-0.367	-0.047	-0.448	-0.128	40.0%
1/4-span	Without creep	-0.106	-	-0.106	-	-
	Fitted model	-0.115	-0.009	-0.128	-0.022	20.8%
	ACI 209 model	-0.117	-0.011	-0.132	-0.026	24.5%
	MC 90 model	-0.118	-0.012	-0.135	-0.029	27.4%
	MC 78 model	-0.119	-0.013	-0.139	-0.033	31.1%

5.3 Stress effect

The stress versus time curves of the steel tube and the core concrete of the steel tube no. 1 at the arch crown are plotted in Figs. 10 and 11. The stress values of the steel tube and the core concrete at finished state and at 3650 days after the bridge is finished are listed in Table 7. In the table, “-” denotes the compressive stress or the increment of the compressive stress, and “+” denotes the tensile stress or reduction of the compressive stress. It can be seen that: (i) the stresses of the CFST section are redistributed due to the creep effect of the core concrete. The stress of the steel tube increases with the increase of time, while the stress of the core concrete has the opposite trend; (ii) the creep stresses of the steel tube and the core concrete calculated by the fitted model are less than by the other three creep models, and the creep stresses obtained by the MC 78 model are the largest among the four models; (iii) by the end of 3650 days after the bridge is finished, the

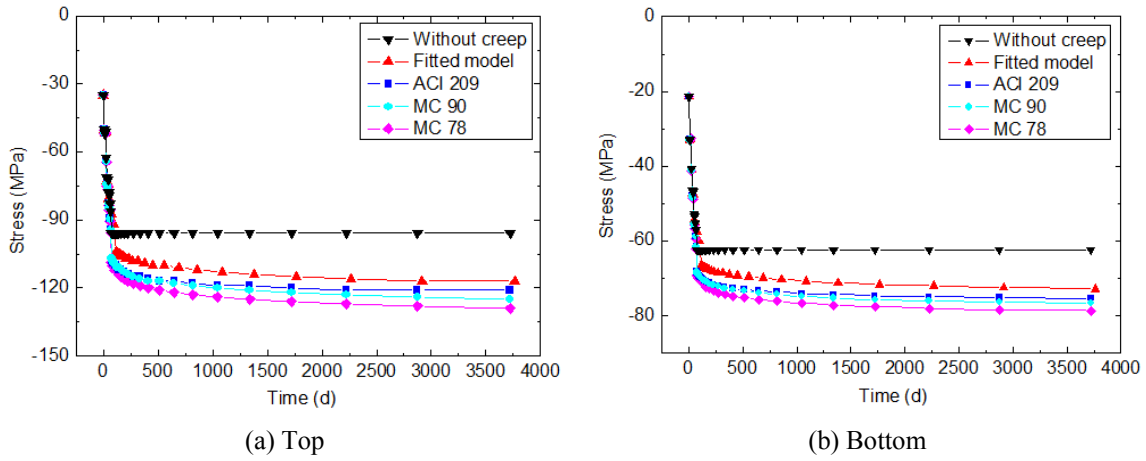


Fig. 10 Stress curves of steel tube at arch crown

top and bottom stresses of the steel tube calculated by the fitted creep model increase by 22.0% and 16.9%, respectively, while the top and bottom stresses of the core concrete decrease by 46.9% and 51.0%, respectively. It is demonstrated that the stress redistribution induced by the creep in the CFST arch bridge is significant, especially for the core concrete stress; (iv) the ratios of the creep stresses after the bridge is finished to the cumulative creep stresses are about 40%~50%, which shows that the creep effect will last for a long time after the CFST arch bridge is finished; (v) the results of the ACI 209 model are the closest to the fitted model, and the differences of the increase ratio by creep between them are less than 5%, demonstrating that the ACI 209 model can be used for creep stress analysis of CFST structures and can meet the engineering accuracy requirement when lack of experimental data.

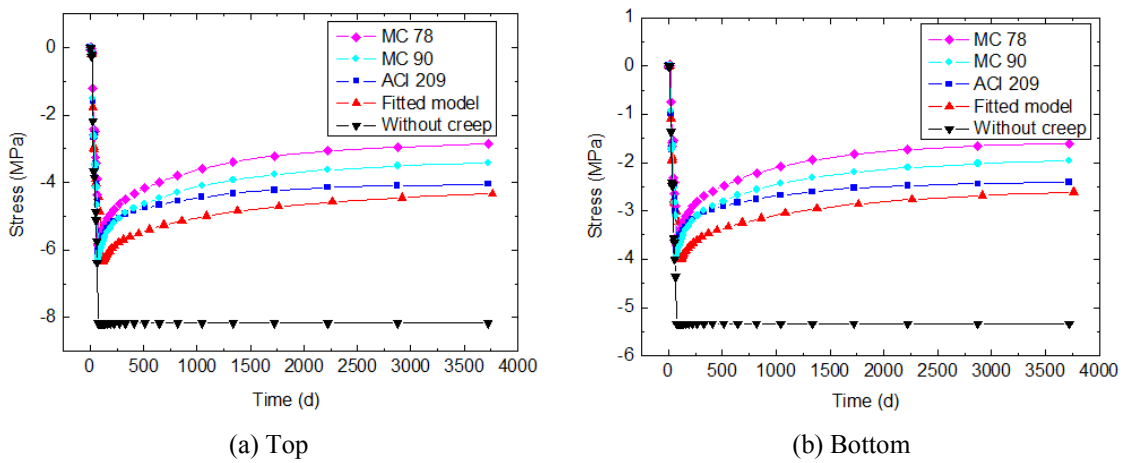


Fig. 11 Stress curves of core concrete at arch crown

Table 7 Stresses of steel tube no. 1 at arch crown for different creep models (unit: MPa)

Element	Position	Creep model	Finished state	Creep stress after finished	3650 days after finished	Cumulative creep stress	Increase ratio by creep
Steel tube	Top	Without creep	-95.9	-	-95.9	-	-
		Fitted model	-104.0	-8.1	-117.0	-21.1	+22.0%
		ACI 209 model	-107.0	-11.1	-121.0	-25.1	+26.2%
		MC 90 model	-107.0	-11.1	-125.0	-29.1	+30.3%
		MC 78 model	-109.0	-13.1	-129.0	-33.1	+34.5%
	Bottom	Without creep	-62.3	-	-62.3	-	-
		Fitted model	-66.6	-4.3	-72.8	-10.5	+16.9%
		ACI 209 model	-68.1	-5.8	-75.3	-13.0	+20.9%
		MC 90 model	-68.3	-6.0	-76.7	-14.4	+23.1%
		MC 78 model	-69.2	-6.9	-78.6	-16.3	+26.2%
Core Concrete	Top	Without creep	-8.16	-	-8.16	-	-
		Fitted model	-6.35	+1.81	-4.33	+3.83	-46.9%
		ACI 209 model	-6.11	+2.05	-4.04	+4.12	-50.5%
		MC 90 model	-6.26	+1.90	-3.41	+4.75	-58.2%
		MC 78 model	-5.88	+2.28	-2.85	+5.31	-65.1%
	Bottom	Without creep	-5.33	-	-5.33	-	-
		Fitted model	-4.00	+1.33	-2.61	+2.72	-51.0%
		ACI 209 model	-3.84	+1.49	-2.41	+2.92	-54.8%
		MC 90 model	-3.97	+1.36	-1.96	+3.37	-63.2%
		MC 78 model	-3.71	+1.62	-1.60	+3.73	-70.0%

6. Conclusions

- (1) This paper first presents the creep experiments of twelve specimens, including nine CFST columns and three plain concrete columns, subjected to three levels of sustained axial loads for 1710 days. The results show that there are some distinctly different creep characteristics between the CFST specimens and the plain concrete specimens. The creep strains of the CFST specimens are far less than those of the plain concrete specimens. The plain concrete creep increases rapidly during the first two years, and then becomes stable, but the concrete creep in the CFST specimens continues to develop after two years.
- (2) In the existing commonly-used models, the creep curves obtained by the ACI 209 model are the closest to the experimental curves of the CFST specimens, indicating that the ACI 209 model outperforms the MC 78 model and the MC 90 model when predicting the creep behavior of the CFST columns. Further, the fitted model based on the ACI 209 model has higher accuracy in representing the creep behavior of the CFST specimens.
- (3) Taking the Maocaojie Bridge as an engineering example, the creep effects of the CFST arch bridge are analyzed and compared, based on the fitted model, the ACI 209 model, the MC 78 model, and the MC 90 model. The results indicate that the creep effects of the

CFST arch bridge are significant. In the three existing models, the results of the ACI 209 model are the closest to the fitted model, and the differences are less than 5%, demonstrating that the ACI 209 model can be used for creep analysis of CFST arch bridges and can meet the engineering accuracy requirement when lack of experimental data.

Acknowledgments

This work was supported by the grants (No. 51378504 and 51229801) from National Natural Science Foundation of China (NSFC), by China Scholarship Council (CSC) and by National Engineering Laboratory for High Speed Railway Construction of Central South University. These supports are greatly appreciated.

References

- Acar, M.H. (2007), "Evaluation of creep coefficient on concrete-filled steel tubular columns", *Indian J. Eng. Mater. Sci.*, **14**(4), 295-302.
- ACI Committee 209 (1992), Prediction of creep, shrinkage and temperature effect in concrete structure (209R-92).
- Bazant, Z.P. and Baweja, S. (1995), "Creep and shrinkage prediction model for analysis and design of concrete structures: Model B3", *Mater. Struct.*, **28**(180), 357-365.
- Bradford, M.A., Pi, Y.L. and Qu, W.L. (2011), "Time-dependent in-plane behavior and buckling of concrete-filled steel tubular arches", *Eng. Struct.*, **33**(5), 1781-1795.
- CEB-FIP (1978), CEB-FIP mode code for concrete structures.
- CEB-FIP (1990), CEB-FIP mode code for concrete structures.
- Chen, Z.H. and Yuan, J.A. (2008), "Creep experimental test and analysis of high-performance concrete in bridge", *J. Central South Univ. Technol.*, **15**(1), 577-581.
- Gardner, N.J. and Lockman, M.J. (2001), "Design provisions for drying shrinkage and creep of normal-strength concrete", *ACI Mater. J.*, **98**(2), 159-167.
- Kim, Y.H., Trejo, D., Hueste, M.B.D. and Kim, J.J. (2011), "Experimental study on creep and durability of high-early-strength self-consolidating concrete for precast elements", *ACI Mater. J.*, **108**(2), 128-138.
- Ma, Y.S. and Wang, Y.F. (2012), "Creep of high strength concrete filled steel tube columns", *Thin-Wall. Struct.*, **53**, 91-98.
- Ma, Y.S., Wang, Y.F. and Mao, Z.K. (2011), "Creep effects on dynamic behavior of concrete filled steel tube arch bridge", *Struct. Eng. Mech., Int. J.*, **37**(3), 321-330.
- Mazloom, M. (2008), "Estimating long-term creep and shrinkage of high-strength concrete", *Cement Concrete Compos.*, **30**(4), 316-326.
- Pan, Z.F., Lü, Z.T. and Fu, C.C. (2011), "Experimental study on creep and shrinkage of high-strength plain concrete and reinforced concrete", *Adv. Struct. Eng.*, **14**(2), 235-247.
- Persson, B. (2001), "Correlating laboratory and field tests of creep in high-performance concrete", *Cement Concrete Compos.*, **31**(3), 389-395.
- Shao, X.D., Peng, J.X., Li, L.F. and Hu, J. (2010), "Time-dependent behavior of concrete-filled steel tubular arch bridge", *J. Bridge Eng.*, **15**(1), 98-107.
- Shrestha, K.M., Chen, B.C. and Chen, Y.F. (2011), "State of the art of creep of concrete filled steel tubular arches", *KSCE J. Civil Eng.*, **15**(1), 145-151.
- Torres, L., Miàs, C., Turon, A. and Baena, M. (2012), "A rational method to predict long-term deflections of FRP reinforced concrete members", *Eng. Struct.*, **40**, 230-239.
- Wang, Y.Y., Geng, Y., Ranzi, G. and Zhang, S.M. (2011), "Time-dependent behavior of expansive

concrete-filled steel tubular columns”, *J. Construct. Steel Res.*, **67**(3), 471-483.
Yang, Y.F., Han, L.H. and Wu, X. (2008), “Concrete shrinkage and creep in recycled aggregate concrete-filled steel tubes”, *Adv. Struct. Eng.*, **11**(4), 383-396.

CC